LASER INTERFEROMETER GRAVITATIONAL WAVE OBSERVATORY
- LIGO -
CALIFORNIA INSTITUTE OF TECHNOLOGY
MASSACHUSETTS INSTITUTE OF TECHNOLOGY

Document Type	**LIGO-T980007-00 - D**	3/2/98

Effect of PO Telescope Aberrations on Wavefront Sensor Performance

Michael Smith

Distribution of this draft:

xyz

This is an internal working note
of the LIGO Project.

California Institute of Technology
LIGO Project - MS 51-33
Pasadena CA 91125
Phone (818) 395-2129
Fax (818) 304-9834
E-mail: info@ligo.caltech.edu

Massachusetts Institute of Technology
LIGO Project - MS 20B-145
Cambridge, MA 01239
Phone (617) 253-4824
Fax (617) 253-7014
E-mail: info@ligo.mit.edu

WWW: http://www.ligo.caltech.edu/

1 INTRODUCTION

This paper will describe the results of a Gaussian beam interference model for analyzing the effects of optical aberrations on the ISC wavefront sensing system (WFS). This model incorporates the use of ASAP optical modeling program to obtain amplitude and phase maps of the sideband and carrier beams at the WFS detector. The modal model, which is normally used to analyze the WFS characteristics, is not readily amenable to describing the effect of complex aberrations due to non-ideal elements in the WFS optical train.

The ISC wavefront sensing system (WFS) detects the misalignment of the various interferometer (IFO) mirrors by measuring the demodulated signal resulting from the interference pattern of the superimposed carrier and two rf modulated sideband beams on a split detector outside the interferometer. The misalignment of a particular mirror will result, in general, in the sideband and carrier beams being displaced and tilted with respect to each other; because the sideband beams resonate only in the recycling cavity, whereas the carrier beam resonates both in the arm cavity and the recycling cavity and tilting a particular mirror will effect the sideband and carrier beams differently at different locations within the IFO. The beams are sampled at various locations within the interferometer by using pick-off (PO) beams reflecting from the back surfaces of the ITM mirrors, from the reflected symmetric port, and from the transmitted anti-symmetric port signals. The interference patterns formed by these PO beams on the surface of the WFS split photodetector provide a measure of the phase difference between the sideband and carrier wavefronts, which in turn carry information related to the misalignment of the interferometer mirrors.

Each PO beam is reduced in diameter by a PO beam telescope and subsequently directed out of the vacuum enclosure through an output window to the ISC WFS system. The wavefront aberrations introduced by the surface irregularities of the PO beam telescope mirrors and associated optical train will affect the performance of the WFS. In order to specify the requirements for the surface figure of the telescope mirrors and the associated optical train, it was necessary to model the degradation of the WFS signal caused by the various optical aberrations.

The WFS optical train is shown schematically in figure 1. It consists of the 7.5X demagnification in-vacuum PO beam telescope, a 3.1X demagnification ISC telescope (for a total beam diameter reduction of 25X), a two-lens Guoy phase telescope, and a split detector.

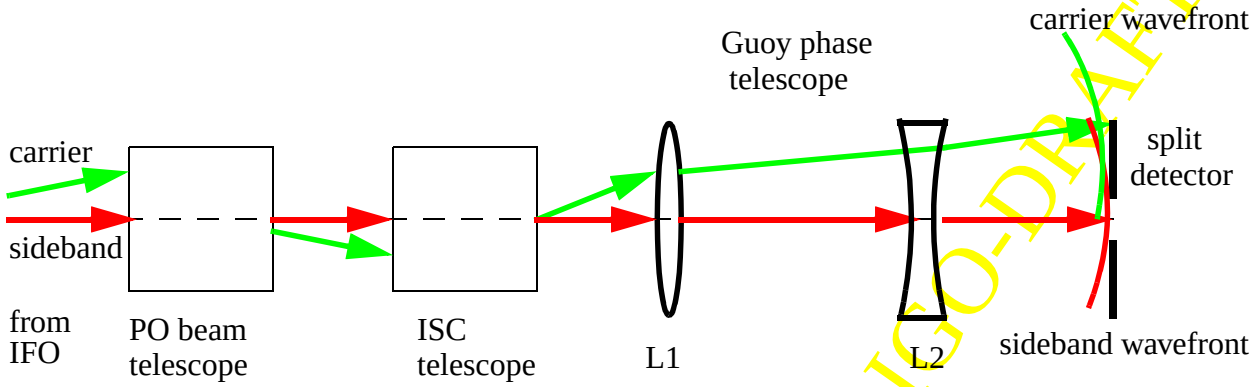

Figure 1: WFS optical train

A detailed schematic of the Guoy phase telescope and WFS detector are shown in figure 2.

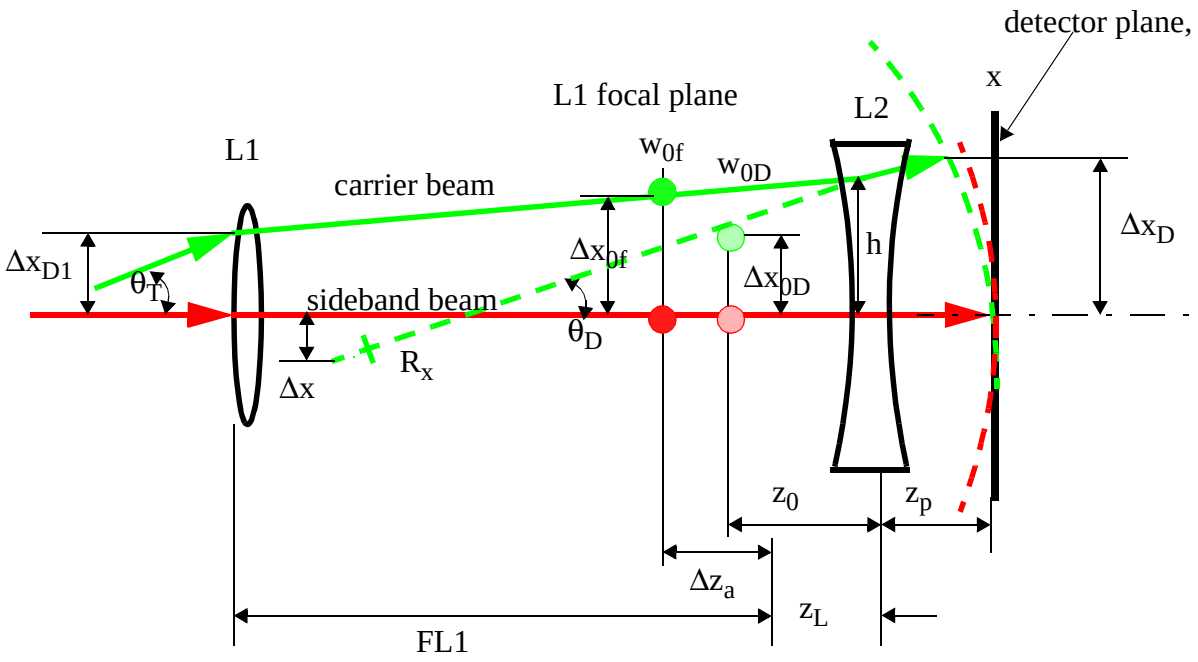

Figure 2: Optical schematic of the WFS displacement sensor

The wavefront sensor is predominately sensitive to relative displacement of the sideband and carrier beams when the second lens of the Guoy telescope is placed at the focal plane of the first Guoy lens, as shown; corresponding to the 90 deg Guoy phase shift position in the modal model. As the L2 is moved away from the focal plane, either towards or away from L1, the wavefront sensor becomes more sensitive to relative tilt of the interfering carrier and sideband beams. Moving toward L1 corresponds to the Guoy phase approaching zero and moving away from L1 corresponds to the Guoy phase approaching 180 deg, in the modal model.

The carrier and sideband spots will interfere coherently across the surface of the photodetector. The on-axis sideband wavefront is centered on the detector and has a phase shift across the detector plane due to the spherical curvature of the wavefront. There will be a phase shift between the sideband and carrier wavefronts due to the relative tilt, displacement, and spherical curvature of the two wavefronts.

Wavefront aberrations in the PO beam telescope will cause additional phase shifts at the detector plane which can mask the phase shifts due to the initial tilt and displacement of the IFO beams. E.g., an astigmatic wavefront aberration imparted by the optical train will be manifested by there being two discrete focal planes along the beam axis at the focus of the first Guoy lens, L1; i.e. different beam waists will occur for two orthogonal directions normal to the beam axis. The best focus occurs midway between the two astigmatic focal planes. Therefore the effect of astigmatism can be described simply as a shift Δz_a in the position of the beam waist away from the nominal

focal plane of the 1st Guoy lens. The focal shift is related to the astigmatic sag of the wavefront, which is proportional to the Zernike astigmatism coefficient A_{022}.

1.1. Analytical-Geometric WFS Model

For the case of astigmatic aberrations only, a rigorous analytical model for the WFS signal can be developed, as follows.

1.1.1. Displacement and Wavefront Curvature of Carrier and Sideband Wavefronts at the Detector Plane

An astigmatic wavefront aberration with maximum wavefront sag equal to the Zernike coefficient A_{022} is imposed across the 100ppm intensity radius of the beam, $2.143w_0$. This will result in an astigmatic focal shift in the x-focal plane given by[1]

$\Delta z_a = 2 \cdot A_{022} \cdot \lambda \cdot \left(\frac{FL1}{M \cdot 2.143 w_0} \right)$. An opposite focal shift will occur in the y-focal plane.

The first Guoy lens L1 creates astigmatic beam waists at the astigmatic focal plane

$w_{ofx} = \frac{1}{\pi} \frac{\lambda (FL1 - \Delta z_a)}{w_0 M}$, $w_{ofy} = \frac{1}{\pi} \frac{\lambda (FL1 - \Delta z_a)}{w_0 M}$, and the Rayleigh ranges associated with these focussed spot widths are

$z_{Rx} = \frac{\pi w_{ofx}^2}{\lambda}$, and $z_{Ry} = \frac{\pi w_{ofy}^2}{\lambda}$.

The lateral displacement and tilt angle of the carrier beam at L2 are determined by the original tilt and displacement of the beam within the interferometer, modified by the magnification and positions of the telescopes in the WFS optical train. A functional relationship is obtained through the use of ABCD matrices, referring to figure 2. The ray height and angle out of L2 are then given by,

$$h = \Delta x_{D1} \left(1 - \frac{FL1 + z_L}{FL1 - \Delta z_a} \right) + \theta_T (FL1 + z_L)$$

$$\theta_D = -\Delta x_{D1} \left[\frac{1}{FL2} \left(1 - \frac{FL1 + z_L}{FL1 - \Delta z_a} \right) + \frac{1}{FL1 - \Delta z_a} \right] - \theta_T \left[\frac{FL1 + z_L}{FL2} - 1 \right].$$

The actual displacement and tilt at the input to L1 and can be expressed in terms of the normalized displacement and tilt of the carrier beam within the interferometer, and the telescopic de- magnification ratio.

$\Delta x_{D1} = \Delta x_0 w_0 M$, and $\theta_T = \frac{\theta_0}{M} \theta_{TIFO}$,

1. Born and Wolfe, Principles of Optics, 6th ed., Pergamon press,1993

where the normalized displacement and tilt are referenced to the IFO beam waist size and diffraction angle respectively:

$\Delta x_0 = \frac{\Delta x_{IFO}}{w_0}$,and $\theta_{TIFO} = \frac{\theta_{IFO}}{\theta_0}$; where $w_0 = 36.4$ mm, and $\theta_0 = \frac{\lambda}{\pi w_0}$ rad.

The second lens L2 of the Guoy phase telescope transforms the carrier and sideband Gaussian beam waists produced by L1 into new virtual beam waists w_{0Dx}, and w_{0Dy} shifted from L2 by the amounts z_{0x}, and z_{0y} with the sideband waists on the optical axis and the carrier waists displaced from the optical axis by Δx_{0Dx}, and:Δx_{0Dy} respectively.

$$z_{0x} = FL2 + \frac{FL2^2 \cdot (\Delta z_a - FL2)}{(\Delta z_a - FL2)^2 + z_R^2},\ z_{0y} = FL2 + \frac{FL2^2 \cdot (-\Delta z_a - FL2)}{(\Delta z_a - FL2)^2 + z_R^2},$$

$$w_{0Dx} = \left[\frac{1}{w_{0fx}^2} \cdot \left(1 - \frac{\Delta z_a + z_L}{FL2}\right)^2 + \frac{1}{FL2^2} \cdot \left(\frac{\pi w_{ofx}}{\lambda}\right)^2\right]^{-\frac{1}{2}},$$

$$w_{0Dy} = \left[\frac{1}{w_{0fy}^2} \cdot \left(1 - \frac{-\Delta z_a + z_L}{FL2}\right)^2 + \frac{1}{FL2^2} \cdot \left(\frac{\pi w_{ofy}}{\lambda}\right)^2\right]^{-\frac{1}{2}}$$

and

$\Delta x_{0Dx} = h + \theta_D \cdot z_{0x}$, $\Delta x_{0Dy} = h + \theta_D \cdot z_{0y}$.

The focal length of L2 is chosen to have a small negative value, so that a negligible increase in Guoy phase will occur after the beam passes through the lens. The detector is placed a distance z_p behind L2 to allow the beam waist to expand to a size commensurate with the detector diameter.

The sideband and carrier spots diverge from the virtual beam waists formed by L2 to larger values w_x and w_y at the detector plane, and acquire wavefront curvatures of radius R_x and R_y.

$$w_x = w_{0Dx} \cdot \left[1 + \left(\frac{\lambda \cdot (z_p - z_{0x})}{\pi w_{0Dx}^2}\right)^2\right]^{\frac{1}{2}}, w_y = w_{0Dy} \cdot \left[1 + \left(\frac{\lambda \cdot (z_p - z_{0y})}{\pi w_{0Dy}^2}\right)^2\right]^{\frac{1}{2}} \text{ and}$$

$$R_x = (z_p - z_{0x}) \cdot \left[1 + \left(\frac{\pi w_{0Dx}^2}{\lambda \cdot (z_p - z_{0x})}\right)^2\right],\ R_y = (z_p - z_{0y}) \cdot \left[1 + \left(\frac{\pi w_{0Dy}^2}{\lambda \cdot z_p - z_{0y}}\right)^2\right].$$

The two spots are displaced at the detector plane by the distance Δx_D,

$\Delta x_D = h + \theta_D \cdot z_p$.

The tilt or displacement of the carrier beam in the IFO causes the center of curvature of the carrier wavefront to be displaced in the x-direction from the sideband center by the amount Δx. The cen-

ter of curvature of the sideband and carrier wavefronts are located to the left of L2, with the sideband center being on the optical axis.

$\Delta x = \Delta x_{0Dx} - \theta_D[R - (z_p - z_{0x})]$.

This separation of the centers of curvature results in a sag Δz between the sideband and carrier wavefronts along the x-axis of the detector plane,

$$\Delta z = \frac{1}{R_x}\left(x \cdot \Delta x - \frac{\Delta x^2}{2}\right).$$

1.1.2. Carrier and Sideband Fields at the WFS Detector, and the WFS Signal

The complex electric fields of the Gaussian carrier and sideband spots at the surface of the detector are given by the following, for a radius of curvature much larger than the spot size:

$$E_C = \frac{E_0}{\sqrt{\pi w_x w_y}} \cdot e^{-\left[\frac{(x-\Delta x_D)^2}{w_x^2} + \frac{y^2}{w_y^2}\right]} \cdot e^{i \cdot \left[\frac{2\pi}{\lambda} \cdot \frac{[(x-\Delta x)^2 + y^2]}{2R_x}\right]}$$

$$E_{SB} = \frac{E_0}{\sqrt{\pi w_x w_y}} \cdot e^{-\left[\left[\frac{x^2}{w_x^2} + \frac{y^2}{w_y^2}\right]\right]} \cdot e^{i \cdot \left[\frac{2\pi}{\lambda} \cdot \frac{(x^2+y^2)}{2R_x} + \frac{\pi}{2}\right]}$$. The $\frac{\pi}{2}$ phase shift of the sideband wavefront is due to the sideband rf modulation.

The two wavefronts interfere coherently on the surface of the WFS photodetector, and the demodulated intensity across the detector is proportional to the square of the sum of the complex fields, $I = E_C \cdot E^{cc}{}_{SB} + E_{SB} \cdot E^{cc}{}_C$; where only the cross product terms give a contribution to the rf demodulated photocurrent. Making a change of variables to a unit radius photodetector, where the Gaussian electric field value at the edge has fallen to 1×10^{-2} of the peak value, $u = \frac{x}{2.143 w_x}$, $v = \frac{y}{2.143 w_y}$, the intensity function across the WFS detector can be written as

$$I = \frac{E^2{}_0}{\pi w_x w_y} \cdot e^{-9.184\left[\frac{u^2}{2} + v^2 + \frac{\left(u - \frac{\Delta x_D}{2.143}\right)^2}{2}\right]} \cdot 2\sin\left[\frac{2\pi}{\lambda} \cdot \frac{(2 \cdot 2.143 u \cdot \Delta x - \Delta x^2)}{2R_x}\right].$$

The first two terms in the argument of the sine function are due respectively to the relative tilt and curvature of the carrier and sideband wavefronts, and are determined primarily by the displacement and tilt of the carrier beam at L1, by the position of L2 beyond the focal plane of L1 (i.e. the Guoy phase position of L2), and to a lesser extent by the focal length of L2 and the position of the detector behind L2.

The WFS signal is obtained by subtracting the integrated intensity across each half of the split photodetector,

$$S = \left(\int_{-1}^{1} \int_{-1}^{0} I(u,v)\,du\,dv - \int_{-1}^{1} \int_{0}^{1} I(u,v)\,du\,dv \right) \cdot 2.143 w_x \cdot 2.143 w_y .$$

The wavefront sensor responds mostly to displacement when L2 is placed at the focal plane of L1, in the near field of the beam waist; i.e. at the position $z_L = 0$. Conversely, the wavefront sensor responds mostly to tilt when L2 is placed some distance away from the focal plane of L1, in the far field of the beam waist; i.e. at $z_L \gg z_R$, where z_R is the Rayleigh range.

1.2. ASAP-Geometric WFS Model

A determination of the effect of non-astigmatic aberrations, such as spherical aberration which destroy the Gaussian characteristic of the beam, on the WFS signal can be obtained by using amplitude/phase maps of the carrier and sideband spots generated by the coherent optical modeling program ASAP. The point by point product of the amplitudes and the phase differences between the sideband and carrier wavefronts can then be integrated numerically over the two halves of the detector plane along either axis and subtracted to obtain the predicted WFS signal.

The electric field distributions for the sideband and carrier beams are calculated by ASAP program and are output in the form of mxn discrete amplitude and phase values for the set of x_m, y_n coordinate sample values. Then the field distributions can be represented as

$$E_C = E_{aC}(x_m, y_n) \cdot e^{i\phi_C(x_m, y_n)},\ E_{SB} = E_{aSB}(x_m, y_n) \cdot e^{i\phi_{SB}(x_m, y_n)},$$

and the intensity across the detector is given by

$$I_{mn} = E_{aC}(x_m, y_n) \cdot E_{aSB}(x_m, y_n) \cdot 2\sin(\phi_C(x_m, y_n) - \phi_{SB}(x_m, y_n)) .$$

The WFS signal integration across the detector can be approximated with a summation over the indices of the spatial map

$$S = \Delta x \Delta y \cdot \left(\sum_{-n}^{n} \sum_{-m}^{0} I_{mn} - \sum_{-n}^{n} \sum_{0}^{m} I_{mn} \right) ,$$

where Δx and Δy are the sampling increments of the spatial map coordinates, and m=0 corresponds to x=0.

1.3. Numerical Results

1.3.1. ASAP WFS Model Results

The PO beam optical train was modeled using ASAP, as shown by the optical schematic layout in figure 3.

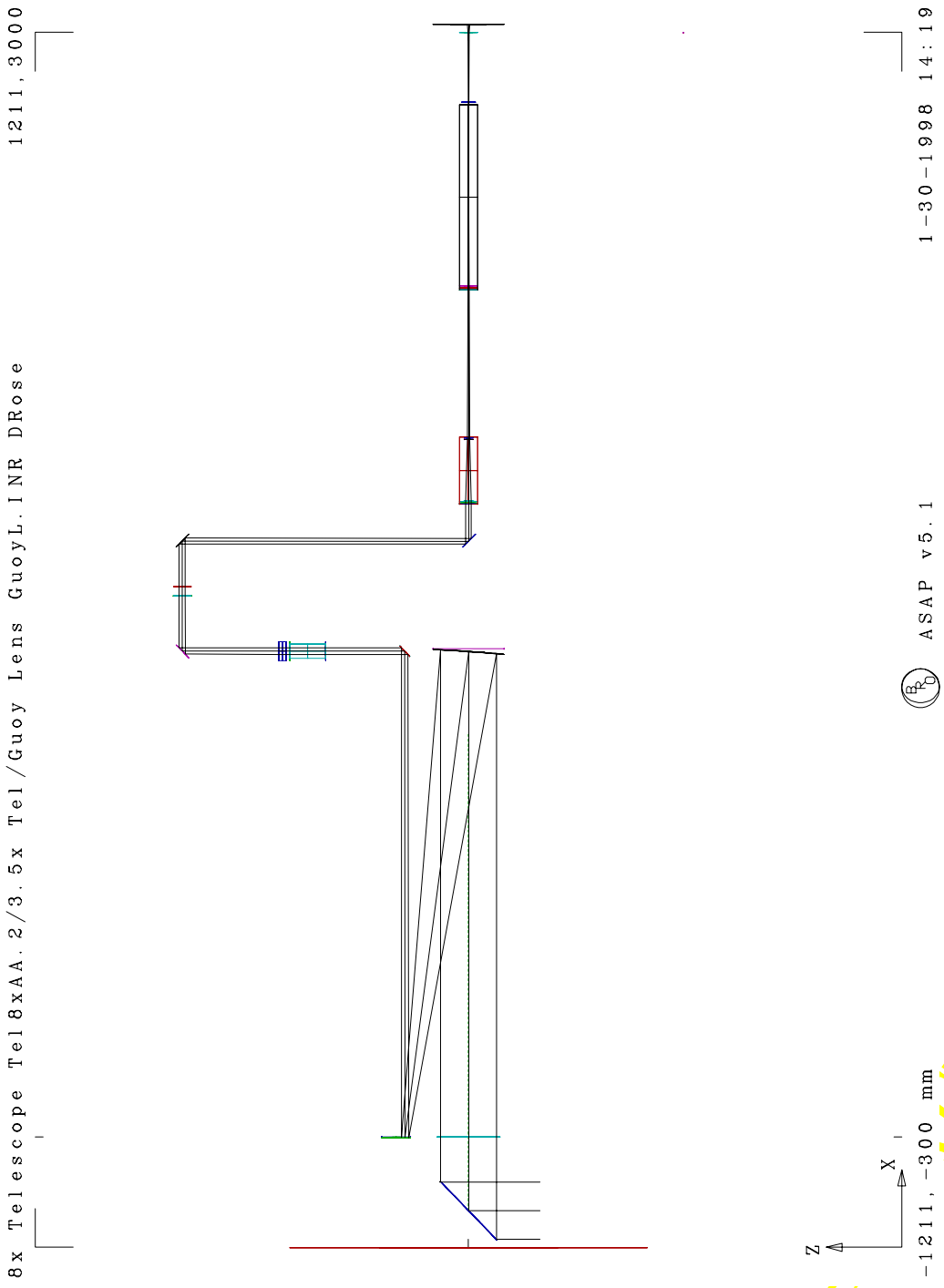

Figure 3: ASAP model of PO beam optical train

The optical train consists of a PO mirror, an 8X demagnification off-axis parabolic reflecting telescope, several turning mirrors, a Faraday isolator with windows, a vacuum output window, a sec-

ond 3.6X demagnification refractive telescope, a 1st Guoy lens, a 2nd Guoy lens, and a detector plane. Individual Zernike polynomial surface distortions were placed on each element.

1.3.1.1 0.9 Waves Astigmatic Aberration

The ASAP-geometric model was used to calculate the WFS signal for the case 0.9λ total spherical aberration on the PO beam optical train. The total aberration was computed by calculating the rms sum of the expected individual aberrations on each element in the optical train. Then, the aberrations were placed on each element using Zernike coefficients in ASAP, and apportioned according to their rms contribution with the requirement that the linear sum of the aberrations in the optical train have the same total as the rms total. The details of the aberration calculations are shown in Table 1 on page 9.

Table 1: Equivalent Surface Sag for Total 0.9 Wave RMS Astigmatic Aberration on the PO Beam Optical Train

	p-v aberration per item	*p-v aberration per item*	*net aberration*	*aberration squared*	*fractional contribution*	*least squares linear equivalent*
	waves @.6328	*waves @ 1.06*				
pick-off mirror	0.250	0.149	0.297	0.088	0.109	0.098
PO telescope, primary	0.500	0.297	0.595	0.354	0.437	0.393
PO telescope, secondary	0.250	0.149	0.297	0.088	0.109	0.098
Faraday Isolator	0.433	0.258	0.258	0.066	0.082	0.074
isolator windows (2)	0.225	0.134	0.189	0.036	0.044	0.040
tel fold mirrors (5)	0.100	0.059	0.266	0.071	0.087	0.079
output window	0.225	0.134	0.134	0.018	0.022	0.020
ISC Telescope, objective	0.250	0.149	0.149	0.022	0.027	0.025
ISC Telescope, eyepiece	0.250	0.149	0.149	0.022	0.027	0.025
Guoy 1st lens	0.250	0.149	0.149	0.022	0.027	0.025
Guoy 2nd lens	0.250	0.149	0.149	0.022	0.027	0.025
sum of squares				0.810	1.000	
total least squares p-v						0.900

The Zernike astigmatism coefficient describes a surface that has a value of sag equal to the coefficient along the x-axis and an equal amount of opposite sag along the y-axis; i.e the measured total p-v sag is exactly twice the value of the coefficient. Therefore the Zernike coefficient should be half the value of the desired p-v sage of the surface. Also, reflective surfaces contribute a total wavefront sag which is twice the value of the surface sag. These factors of two were taken into account when the total modeled aberration was apportioned among the elements in the optical train. The actual astigmatic Zernike coefficient values placed on the optical elements to produce a total 0.9 wave p-v added in an rms manner are shown in Table 2 on page 10

Table 2: Equivalent Linear Astigmatic Zernike Coefficients for a Total 0.9 Wave RMS Aberration on the PO Beam Optical Train

element	*equivalent Zernike aberration on surface*
	waves @ 1.06
pick-off mirror	-0.025
PO telescope, primary	0.098
PO telescope, secondary	-0.025
Faraday Isolator	-0.037
isolator windows (2)	-0.020
tel fold mirrors (5)	-0.020
output window	-0.010
ISC Telescope, objective	-0.012
ISC Telescope, eyepiece	-0.012
Guoy 1st lens	-0.012
Guoy 2nd lens	0.012
total least squares p-v	0.900

ASAP amplitude and phase data files were obtained for a range of Guoy phase values with 0.01 normalized displacement and 0.01 normalized tilt of the carrier beam within the IFO. Two data sets were obtained, with +0.9 waves astigmatic aberration to represent the x-axis signal and with -0.9 waves astigmatic aberration to represent the y-axis.

A typical carrier and sideband amplitude product with +0.9 waves astigmatism for a normalized carrier displacement of 0.01 at 135 deg Guoy phase is shown in figure 4.

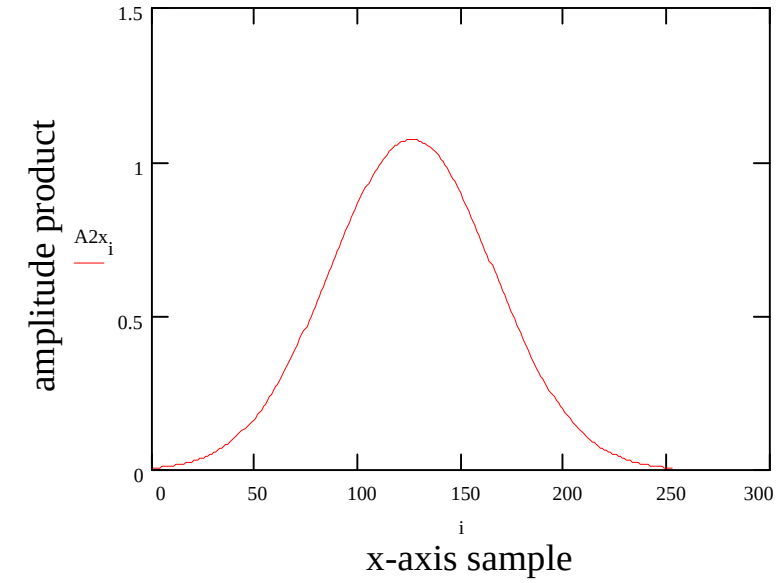

Figure 4: Carrier and Sideband Amplitude Product at 135 deg Guoy Phase, for 0.01 Displacement, 0.9 Wave RMS Astigmatic Aberration

A typical carrier and sideband wavefront phase difference for a normalized carrier displacement of 0.01 at 135 deg Guoy phase is shown in figure 5.

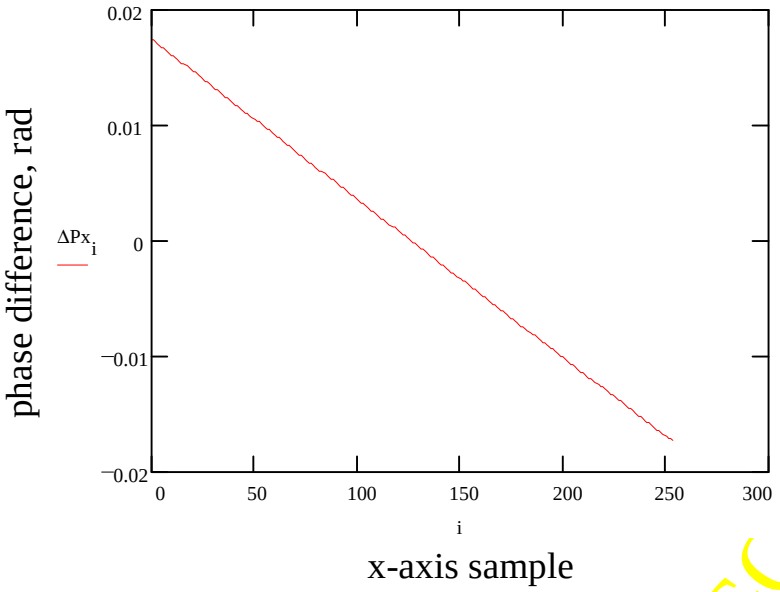

Figure 5: Carrier and Sideband Wavefront Phase Difference at 135 deg Guoy Phase, for 0.01 Displacement, 0.9 Wave RMS Astigmatic Aberration

A typical carrier and sideband intensity distribution across the WFS detector for a normalized carrier displacement of 0.01 at 135 deg Guoy phase is shown in figure 6.

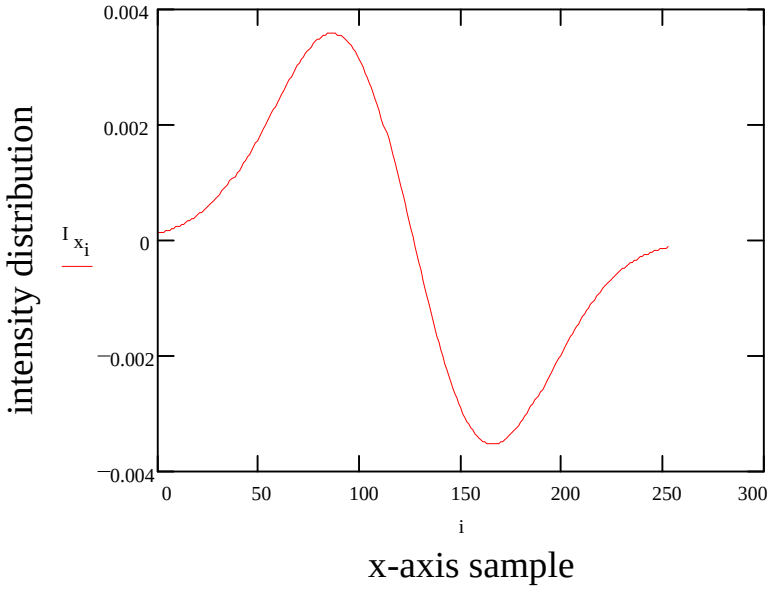

Figure 6: Carrier and Sideband Intensity Distribution at 135 deg Guoy Phase, for 0.01 Displacement, 0.9 Wave RMS Astigmatic Aberration

A contour profile of the intensity distribution across the WFS detector for a normalized carrier displacement of 0.01 at 135 deg Guoy phase is shown in figure7. There is a slight amount of cross-coupling of the x-axis tilt into the y-axis signal. However, the tilt component in the y-axis is negligible compared to the x-axis. The intensity distribution has the characteristics of the product of a TEM10 and TEM00 Gaussian modes, as predicted by the WFS modal model.

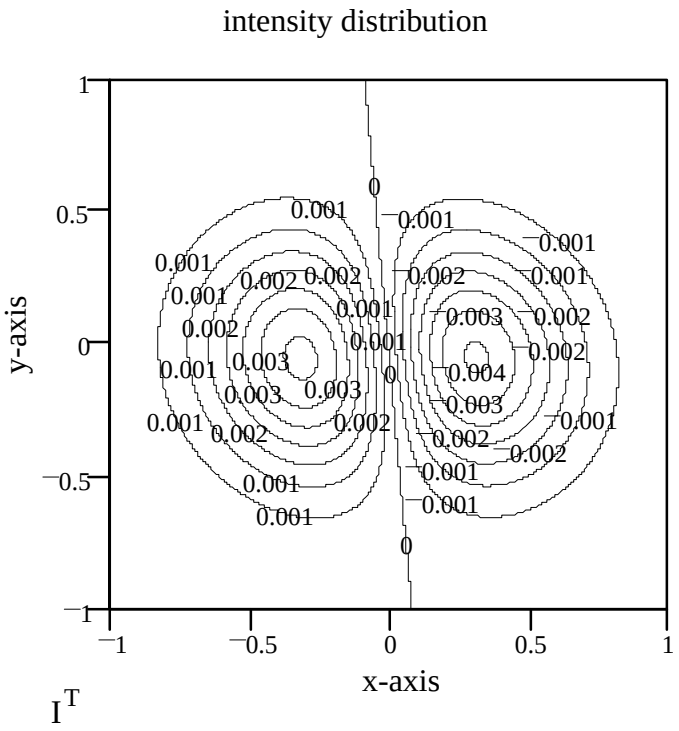

Figure 7: Carrier and Sideband Wavefront Intensity Map at 135 deg Guoy Phase, for 0.01 Displacement, 0.9 Wave RMS Astigmatic Aberration

A summary of the displacement and tilt WFS signals for various Guoy phases with +0.9 waves astigmatism and -0.9 waves astigmatism are shown in figures 8 and 9. The individual data points are connected with straight lines in all of the figures for clarity.

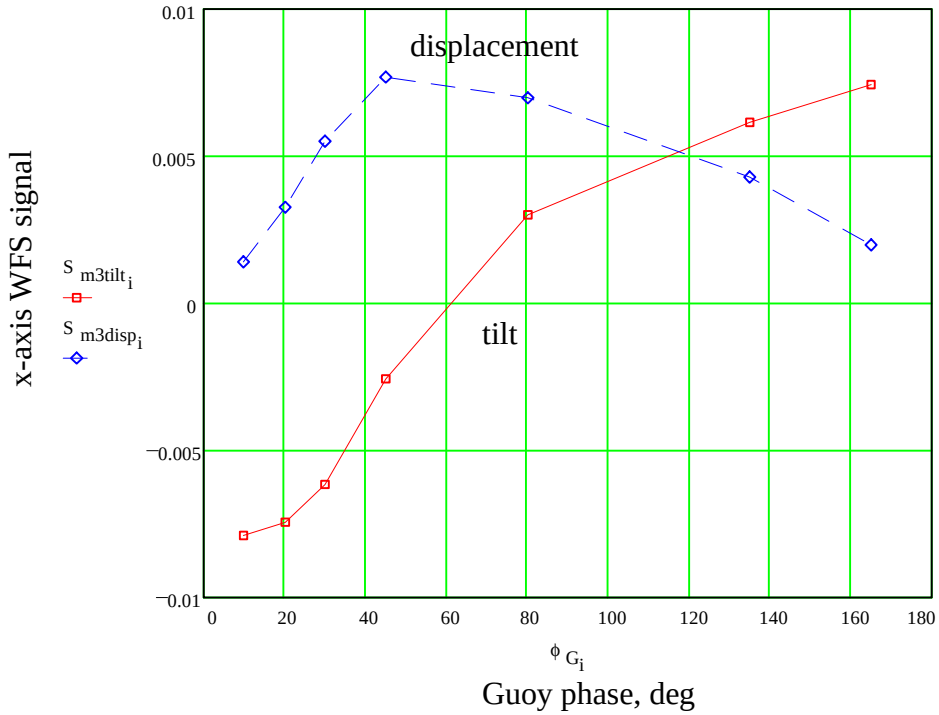

Figure 8: Summary of WFS signals versus Guoy phase for 0.01 displacement and 0.01 tilt, with +0.9 waves astigmatism

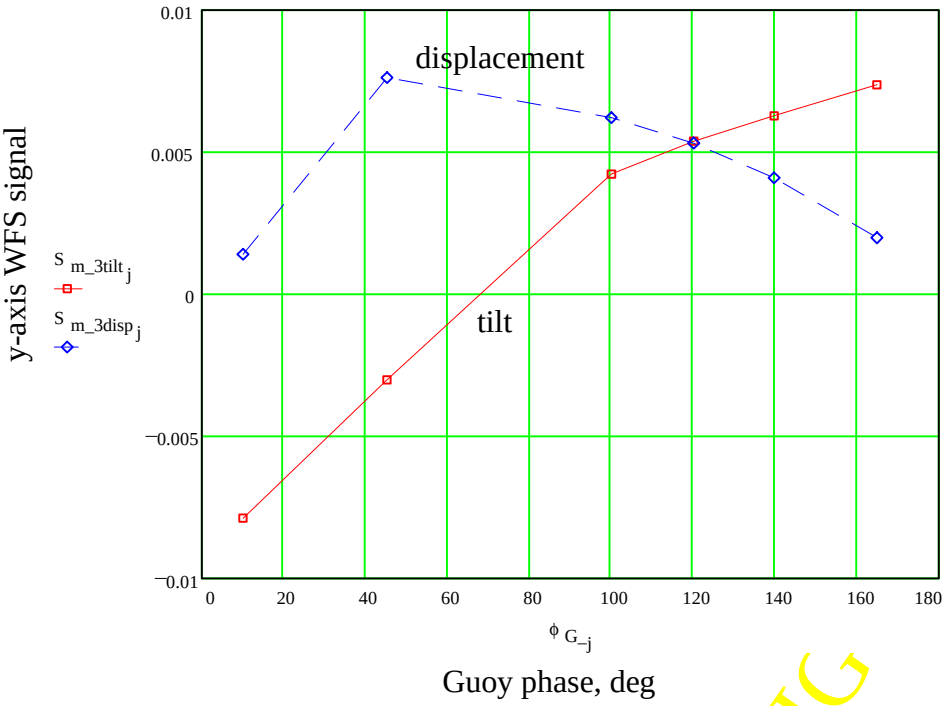

Figure 9: Summary of WFS signals versus Guoy phase for 0.01 displacement and 0.01 tilt, with -0.9 waves astigmatism

The +0.9 waves aberration relates to the x-axis signal, and the -0.9 waves aberration relates to the y-axis signal.

The optimum Guoy phase location for placing a tilt or displacement detector can be determined by calculating the tilt or displacement signal cross-coupling ratios.

$R_D = \frac{S_{disp}}{S_{tilt}}$, and $R_T = \frac{S_{tilt}}{S_{disp}}$. The tilt cross-coupling ratio should be >5 to unambiguously detect tilt, and likewise the displacement cross-coupling ratio should be >5 to detect displacement; according to ASC requirements.

The cross-coupling ratios for tilt detection and displacement detection for the x-axis and y-axis are shown in figures 10 and 11, where the smooth curves were calculated by fitting the best cubic spline function to the discrete data points. It can be seen that the same ratios have peaks occurring at different Guoy phases for the x-axis and y-axis.

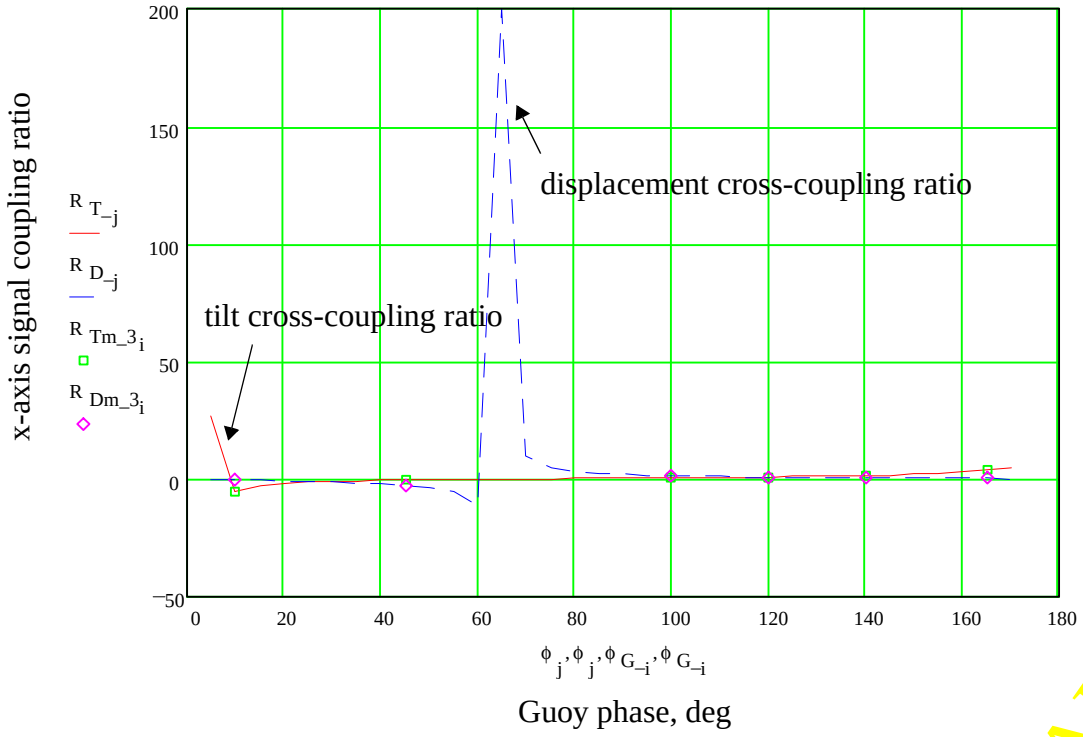

Figure 10: X-axis cross-coupling ratios for tilt and displacement, 0.9 waves astigmatism

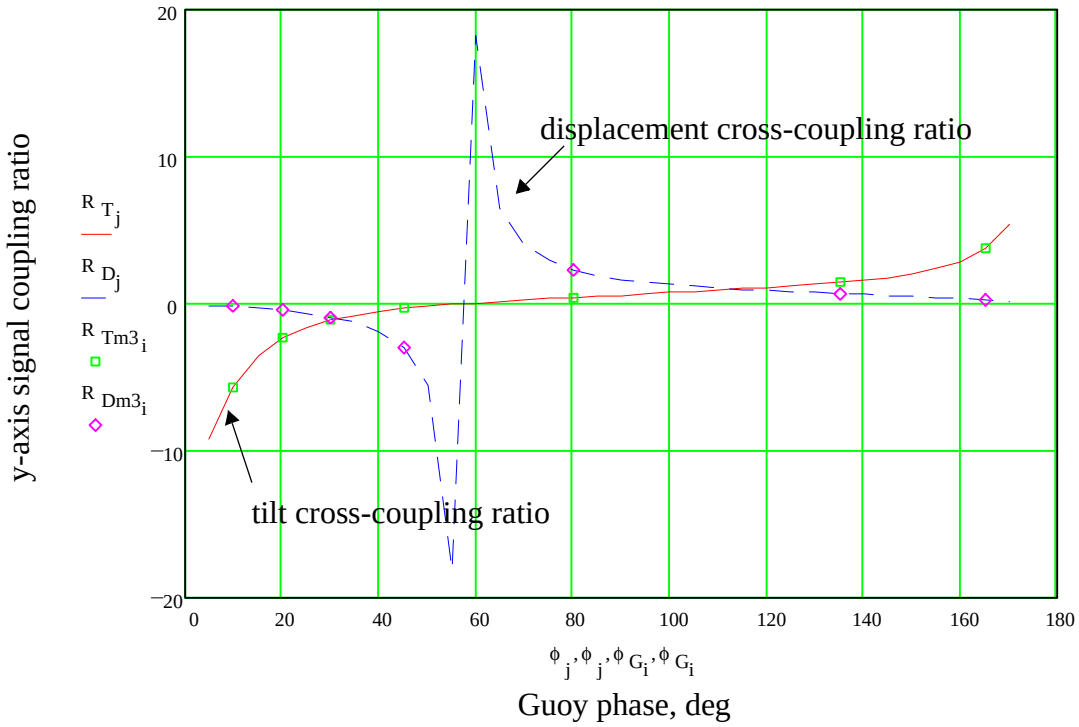

Figure 11: Y-axis cross-coupling ratios for tilt and displacement, 0.9 waves astigmatism

A tilt signal contrast ratio of >5 can be obtained in both axes by placing the tilt detector at 5 deg Guoy phase. Similarly, a displacement signal contrast ratio of >5 can be obtained in both axes by placing the displacement detector at 65 deg Guoy phase.

1.3.1.2 0.98 Waves Spherical Aberration with 1.3 m PO telescope

The ASAP-geometric model was used to calculate the WFS signal for the case 0.98λ total spherical aberration on the PO beam optical train using a 1.3 m PO telescope. The details of the aberration calculations are shown in Table 3 on page 17. The actual spherical Zernike coefficient values placed on the optical elements to produce a total 0.98 wave p-v added in an rms manner are shown in Table 4 on page 18.

The signal contrast ratios for tilt detection and displacement detection for the x-axis and y-axis are shown in figures 12 and 13, where the smooth curves were calculated by fitting the best cubic spline function to the discrete data points. It can be seen that the same ratios have peaks occurring at different Guoy phases for the x-axis and y-axis.

A tilt signal contrast ratio of >5 can be obtained in both axes by placing the tilt detector at 5 deg Guoy phase. Similarly, a displacement cross-coupling ratio of >5 can be obtained in both axes by placing the displacement detector at 65 deg Guoy phase.

Table 3: Equivalent Surface Sag for Total 0.98 Wave RMS Spherical Aberration on the 1.3m PO Beam Optical Train

	p-v aberration per item	*p-v aberration per item*	*net aberration*	*aberration squared*	*fractional contribution*	*least squares linear equivalent*
	waves @.6328	*waves @ 1.06*				
pick-off mirror	0.464	0.276	0.552	0.305	0.320	0.312
PO telescope, primary	0.232	0.138	0.276	0.076	0.080	0.078
PO telescope, secondary	0.232	0.138	0.276	0.076	0.080	0.078
Faraday Isolator	0.509	0.303	0.303	0.092	0.096	0.094
isolator windows (2)	0.209	0.124	0.176	0.031	0.032	0.032
tel fold mirrors (7)	0.186	0.110	0.584	0.341	0.358	0.350
output window	0.209	0.124	0.124	0.015	0.016	0.016
ISC Telescope, objective	0.105	0.062	0.062	0.004	0.004	0.004
ISC Telescope, eyepiece	0.105	0.062	0.062	0.004	0.004	0.004
Guoy 1st lens	0.105	0.062	0.062	0.004	0.004	0.004
Guoy 2nd lens	0.105	0.062	0.062	0.004	0.004	0.004
sum of squares				0.952	1.000	0.976
least squares p-v						0.976

Table 4: Equivalent Linear Spherical Zernike Coefficients for a Total 0.98 Wave RMS Aberration on the 1.3m PO Beam Optical Train

	equivalent Zernike aberration on surface
	waves @ 1.06
pick-off mirror	-0.156
PO telescope, primary	0.039
PO telescope, secondary	-0.039
Faraday Isolator (note1)	-0.094
isolator windows (2)	-0.032
tel fold mirrors (7)	-0.175
output window	-0.016
ISC Telescope, objective	-0.004
ISC Telescope, eyepiece	-0.004
Guoy 1st lens	-0.004
Guoy 2nd lens	0.004
least squares p-v	0.976

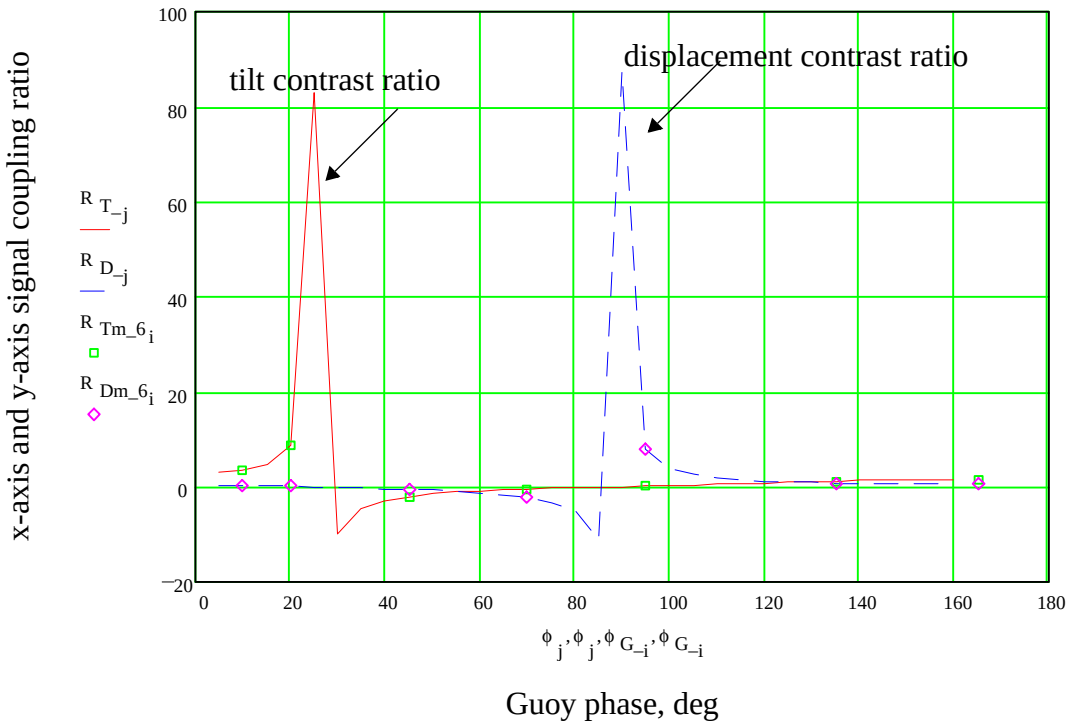

Figure 12: X,Y-axis contrast ratios for tilt and displacement, 0.98 wave spherical aberration

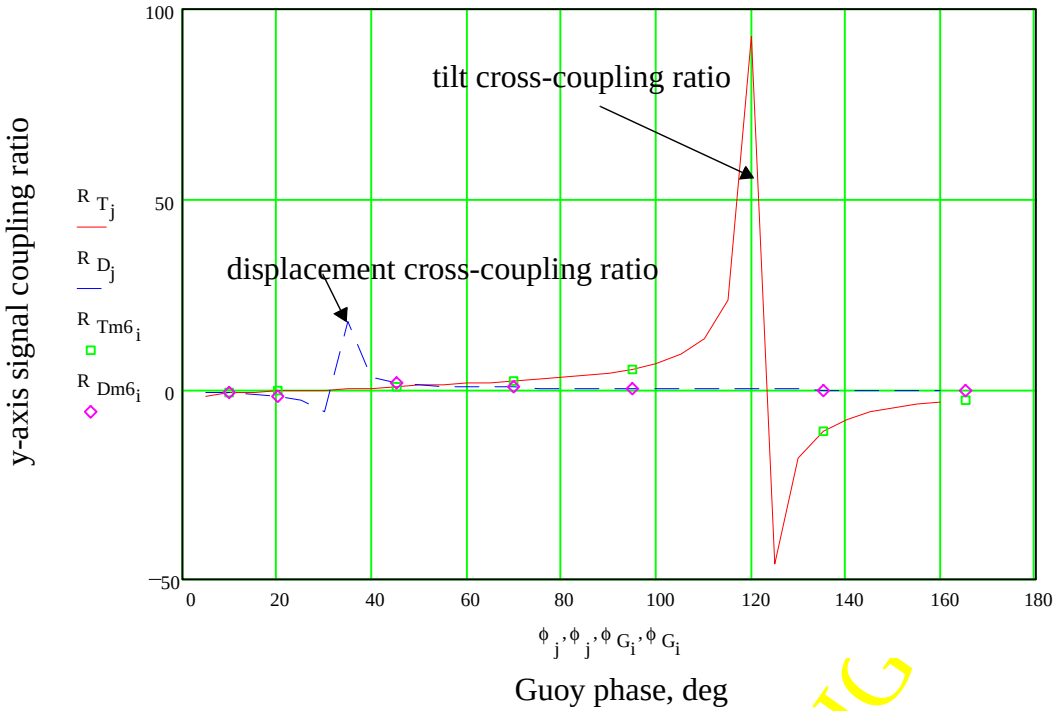

Figure 13: X,Y-axis cross-coupling ratios for tilt and displacement, 0.98 wave spherical aberration

1.3.2. Comparison of ASAP WFS Model with Analytical WFS Model

In order to test the validity of the ASAP WFS model a comparison was made with the analytical WFS for astigmatic aberrations only.

The following parameters were chosen for the analytical model:

spot radius in the IFO, $w_0 = 36.4\,\text{mm}$

wavelength, $\lambda = 1.06\times10^{-3}\,\text{mm}$

IFO Rayleigh angle, $\theta_0 = 9.3\times10^{-6}\,\text{rad}$

de-magnification of telescope, $M = 0.035$

normalized beam tilt, $\theta_{TIFO} = -0.01$

normalized beam displacement, $\Delta x_0 = -0.01$

Zernike x-astigmatism coefficient, $A_{022} = 0.5\ \lambda$,

note that this coefficient is equivalent to1.0 waves of aberration.

focal length 1st Guoy lens, $FL1 = 503\,\text{mm}$

focal length 2nd Guoy lens, $FL2 = -50\,\text{mm}$

beam tilt at 1st Guoy lens, $\theta_T = \frac{\theta_0}{M}\cdot\theta_{TIFO}\ \text{rad}$

beam displacement at 1st Guoy lens $\Delta x_{D1} = \Delta x_0 \cdot w_0 \cdot M\ \text{mm}$

The total energy in the analytical model, which is proportional to the integrated product of the sideband and carrier field amplitudes, was set equal to unity; the same integrated energy value used by the ASAP program.

The analytical WFS model results are shown as curved lines. The ASAP model data points have been superimposed. There is excellent agreement at the endpoints of the curves, and the ASAP model data points follow the trends indicated by the analytical model.

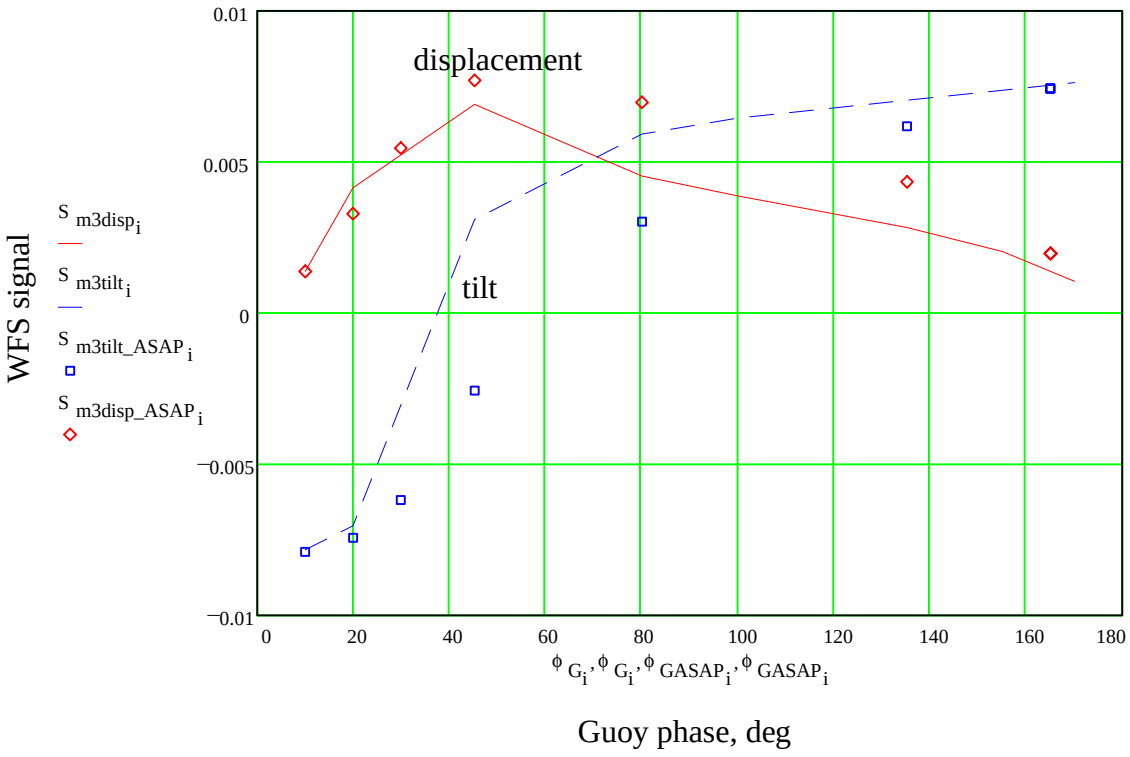

Figure 14: Comparison of analytical WFS analysis with the ASAP WFS model results

1.3.3. Requirements for Wavefront Aberrations in the PO Beam Optical Train

Based on the results of the ASAP WFS model, it appears conservative to specify that the displacement/tilt cross-coupling ratio and the tilt/displacement cross-coupling ratio of the WFS signals at the orthogonal Guoy phase positions for detecting displacement and tilt shall be >5:1. With cross-coupling ratios >5:1, an unambiguous determination of the magnitudes of the tilt and displacement values can be obtained by inverting the tilt-displacement signal matrix.

These requirements on the cross-coupling ratios imply a maximum allowed total rms aberration on the PO beam optical train of <1 wave @ 6328 wavelength. The aberrations can be either purely astigmatic or purely spherical. We will assume that any combination of astigmatism and spherical with a total rms value <1 wave is acceptable. In fact, an ASAP WFS data run with 0.45 waves astigmatism and 0.225 waves spherical exhibited satisfactory cross-coupling ratios.